Low-emittance thermionic-gun-based injector for a compact free-electron laser

Takao Asaka,[1] Hiroyasu Ego,[1,2] Hirohumi Hanaki,[2] Toru Hara,[1] Taichi Hasegawa,[3] Teruaki Hasegawa,[1] Takahiro Inagaki,[1] Toshiaki Kobayashi,[2] Chikara Kondo,[1] Hirokazu Maesaka,[1] Shinichi Matsubara,[2] Sakuo Matsui,[1] Takashi Ohshima,[1] Yuji Otake,[1] Tatsuyuki Sakurai,[2] Shinsuke Suzuki,[2] Yasuyuki Tajiri,[3] Shinichiro Tanaka,[3] Kazuaki Togawa,[1] and Hitoshi Tanaka[1]

[1]*RIKEN SPring-8 Center, Kouto 1-1-1 Sayo, Hyogo 679-5148, Japan*
[2]*Japan Synchrotron Radiation Research Institute (JASRI), Kouto 1-1-1 Sayo, Hyogo 679-5198, Japan*
[3]*SPring-8 Service Company Limited, Kouto 1-20-5, Shingu-cho, Tatsuno, Hyogo 679-5165, Japan*

(Received 28 December 2016; revised manuscript received 12 May 2017; published 14 August 2017)

A low-emittance thermionic-gun-based injector was developed for the x-ray free-electron laser (XFEL) facility known as the SPring-8 angstrom compact free-electron laser (SACLA). The thermionic-gun-based system has the advantages of maintainability, reliability, and stability over a photocathode radio-frequency (rf) gun because of its robust thermionic cathode. The basic performance of the injector prototype was confirmed at the SPring-8 compact self-amplified spontaneous emission source (SCSS) test accelerator, where stable FEL generation in an extreme ultraviolet wavelength range was demonstrated. The essential XFEL innovation is the achievement of a constant beam peak current of 3–4 kA, which is 10 times higher than that generated by the SCSS test accelerator, while maintaining a normalized-slice emittance below 1 mm mrad. Thus, the following five modifications were applied to the SACLA injector: (i) a nonlinear energy chirp correction; (ii) the optimization of the rf acceleration frequency; (iii) rf system stabilization; (iv) nondestructive beam monitoring; and (v) a geomagnetic field correction. The SACLA injector successfully achieved the target beam performance, which shows that a thermionic-gun-based injector is applicable to an XFEL accelerator system. This paper gives an overview of the SACLA injector and describes the physical and technical details, together with the electron beam performance obtained in the beam commissioning.

DOI: 10.1103/PhysRevAccelBeams.20.080702

I. INTRODUCTION

The intense coherent x-ray beams generated by an x-ray free-electron laser (XFEL) are an extremely powerful tool for conducting groundbreaking experiments on the fundamental processes of chemistry, material science, and biology. The SPring-8 angstrom compact free-electron laser (SACLA) is the world's first compact XFEL facility [1] based on the SPring-8 compact self-amplified spontaneous emission (SASE) source (SCSS) concept [2,3], which targets the generation of stable and short-wavelength XFEL lights in a compact facility. Short-period in-vacuum undulator technology [4] reduces the electron beam energy necessary for XFEL, and a C-band acceleration system [5] shortens the accelerator length via its high-gradient acceleration fields. As the emittance damping effect is reduced with decreased beam energy, a small normalized-slice emittance below 1 mm mrad at the injector is required for this setup to function effectively.

In SACLA, a single crystal thermionic cathode is employed, which yields stable emission and has a long lifetime compared to the photocathode used in radio-frequency (rf) guns [6]. However, since the peak current of the electron beam emitted from the thermionic cathode is low, velocity bunching inside the injector section is necessary [7].

The SCSS test accelerator was constructed as a SACLA prototype in 2004–2005 [8]. The majority of the accelerator components used in SACLA were tested in a test accelerator, such as a 40-MeV injector prototype, a single magnetic bunch compressor, C-band accelerators, in-vacuum undulators, and beam diagnostics. The validity of the SCSS concept was proven via the successful operation of the SASE FEL at a 49-nm wavelength in 2006 [9]. The electron-bunch peak current reached 300 A with a normalized-slice emittance of 0.7 mm mrad at 250 MeV [10,11].

The SACLA injector was subsequently designed based on the SCSS injector. To reach the total bunch compression factor of approximately 3000 and the required peak current of 3–4 kA for XFEL, substantial modifications were implemented, as summarized below.

(i) *Nonlinear energy chirp correction for bunch compression processes.*—To compress the bunch by a factor of 3000 while maintaining its low emittance, bunch-process linearization is indispensable. Further, overbunching should be avoided. To linearize the bunch energy chirp, two harmonic rf cavities were installed in the SACLA injector. An L-band rf cavity linearizes the energy chirp during the velocity bunching process. The appropriate energy chirp at the injector exit is formed by a C-band rf cavity, so that a peak current of 3 kA is obtained after the magnetic bunch compressors, without overbunching.

(ii) *Optimization of accelerating rf frequency.*—The S-band structure used in the SCSS injector was changed to an L-band accelerating structure in SACLA. This frequency change is critically important for introducing a "simple nonlinear chirp correction scheme" with no X-band correction cavity [12]. In addition, the superfluous satellite bunches that were generated in the previous S-band structure became negligible in the L-band structure implemented in SACLA because of its wide acceptance.

(iii) *rf-system stabilization.*—To suppress the peak current fluctuation after the magnetic bunch compressors to within 10% (standard deviation; std), stabilities of 100 ppm (std) and less than 100 fs (std) are required for the rf amplitude and phase, respectively. In order to achieve these targets, we eliminated various sources of instability, i.e., the electric power variation, temperature change, and mechanical vibration.

(iv) *Nondestructive beam diagnostic system for precise parameter monitoring.*—During injector beam commissioning, it is important to measure the beam parameters. We have developed a high-accuracy real-time diagnostic system, incorporating an electron-beam arrival timing monitor.

(v) *Installation of long coils for geomagnetic field correction.*—The majority of beam tuning processes are based on the projected emittance. Therefore, in order to achieve smooth beam tuning, it is important to achieve the smallest possible difference between the projected and slice emittances. When a low-energy electron beam is deflected by the geomagnetic field, chromatic dispersion is caused, which increases the projected emittance. To avoid this deterioration, air coils were used to compensate for the geomagnetic field in SACLA.

In this paper, an overview of the SACLA injector is provided. The physical and technical details of the injector are also described, together with the electron beam performance obtained during the beam commissioning. In Sec. II, the SACLA injector configuration is outlined. Then, the methods and hardware employed in the modifications (compared to the SCSS) are explained in detail in Sec. III. In Sec. IV, the measurement results of the beam performance at the end of the injector, such as the peak current, projected emittance, and energy profile, are compared with a particle tracking simulation to ensure that the design parameters are appropriately set in the real injector. We found that the short-term laser-pointing stability was strongly correlated with the electron beam orbit inside the injector. The source of this instability and a method of overcoming this problem are described.

II. SACLA 30-MEV INJECTOR CONFIGURATION

The SACLA light source is composed of a 400-m-long 8-GeV linear accelerator [13], a beam switchyard, beam transport lines, and five undulator beam lines, three of which have been installed, as shown in Fig. 1. The linear accelerator consists of a 30-MeV injector followed by the first magnetic bunch compressor, BC1, S-band and C-band accelerating sections providing the required energy chirps for the second and third magnetic bunch compressors (BC2 and BC3, respectively), and the main acceleration section. The linear accelerator provides a bunched beam having a peak current of 3 kA or higher, a bunch length of a few tens of femtoseconds, and a normalized-slice emittance of less than 1 mm mrad. The main beam parameters of the 8-GeV linear accelerator are summarized in Table I, and the layout of the 30-MeV injector is shown in Fig. 2.

In the injector, the electron beams are emitted from a CeB_6 thermionic cathode of 3-mm diameter with a 500-kV voltage at a 3-μs pulse width [14]. The beam chopper after the gun cuts a short pulse of 1 ns from a microsecond beam. The chopper collimator removes the superfluous electrons emitted from the cathode edge and the inhomogeneous halo to form a cylindrical uniform beam pulse, which has a peak current of 1 A with a low emittance of 0.6 mm mrad. Because of the electron beam homogeneity, the emittance is ideally conserved, with no nonlinear space-charge force. The linear space-charge forces are balanced using magnetic lenses, and the extracted electron beam is compressed by the velocity bunching system.

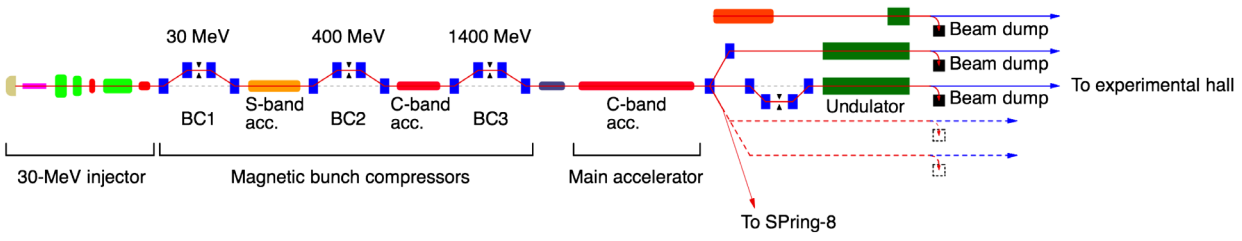

FIG. 1. Schematic view of the 8-GeV linear accelerator and undulator section of SACLA.

TABLE I. SACLA 8-GeV linear accelerator (linac) beam parameters.

Parameter	Unit	Design	Measurement
Final injector e^- energy	MeV	30	30
BC1 e^- energy	MeV	30	30
BC2 e^- energy	MeV	400	400
BC3 e^- energy	GeV	1.4	1.4
End of linac energy	GeV	8	8
Slice energy spread	%	0.004	⋯
Energy stability	%	0.01	0.01
Gun bunch charge	nC	1.3	1.3
Final injector bunch charge	nC	0.7	0.7
BC1 bunch charge	nC	0.3	0.3
End of linac bunch charge	nC	0.3	0.3
Beam chopper bunch length (FWHM)	ns	1.2	1.2
Final injector bunch length (FWHM)	ps	9	8.8
Final injector peak current	A	20	25
End of linac peak current	kA	3	>3
Normalized projected emittance	mm mrad	1/1	1.1/1.1
Repetition rate	Hz	60	1–60

A 238-MHz subharmonic buncher (SHB) is used to efficiently capture the 1-ns electron beam and to generate the energy chirp over the beam. In fact, the SHB decelerates the electron beam so as to suppress the second-order nonlinearity of the relationship between the beam energy and its velocity. Thus, the beam energy decreases from 500 to 400 keV. The velocity-modulated electron beam is compressed to less than 20 ps before reaching the L-band accelerator. In the bunching process, to avoid the space-charge effect, the beam is accelerated up to 1 MeV by a 476-MHz booster cavity, which is located between the 238-MHz SHB and the L-band accelerator. The peak current further increases to 20 A at the end of a 2-m drift section located downstream of the booster cavity. Then, two L-band accelerating structures, which are positioned at the end of the injector, accelerate the beam to the ultrarelativistic energy range. The velocity bunching process is completed in the first L-band structure. The beam energy reaches approximately 35 MeV at the exit of the L-band accelerating structure. Simultaneously, the off-crest acceleration generates the energy chirp required by the first magnetic bunch compressor.

After the injector, the three-stage magnetic bunch compressor compresses the electron beam to a final bunch length of 30 fs or less, and the C-band main acceleration system boosts the beam energy to 8 GeV, which is the SACLA design value.

III. INJECTOR UPGRADES FOR PRODUCING A STABLE, HIGH-INTENSITY, LOW-EMITTANCE BEAM

A. Nonlinear energy chirp correction in bunch compression processes using harmonic rf cavities

To obtain a peak current of more than 3 kA corresponding to a compression factor of more than 3000, the bunch length is shortened using two methods: velocity bunching and magnetic bunch compression. Note that, for such extreme compression, the energy chirp nonlinearity restricts the attainable compression factor. Overbunching easily occurs before the target compression factor is obtained; hence, the slice emittance deteriorates. To avoid this overbunching phenomenon, two harmonic rf cavities were installed in the SACLA injector.

In the velocity bunching process, the bunch energy is modulated so that the tail electrons, which have greater velocity, catch the head electrons following traversal of the drift space [7]. In order to compensate for the second-order nonlinearity, an L-band correction rf cavity was installed immediately after the 476-MHz booster cavity. The correction-cavity phase was set to a deceleration phase. Using the PARMELA particle tracking simulation code, it was confirmed that the bunch length at the buncher section could be shortened to 15 ps (full width at half maximum; FWHM) without overbunching, as shown in Fig. 3.

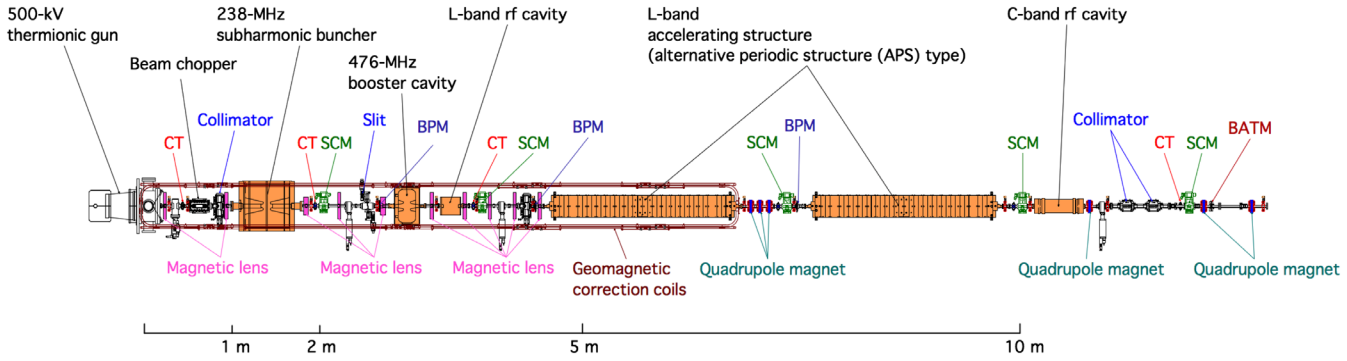

FIG. 2. Layout of the SACLA 30-MeV injector. The injector is equipped with various beam monitors: a current-transformer-type beam charge monitor (CT), a screen monitor (SCM), a strip-line-type beam position monitor (BPM), and a beam arrival time monitor (BATM).

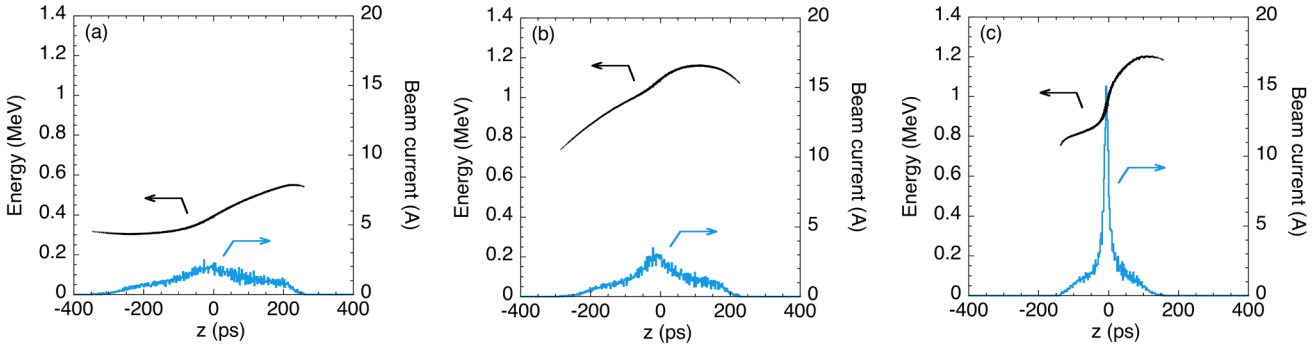

FIG. 3. Energy profile (black dots) and beam current (blue line) as functions of the bunch longitudinal position (time), simulated using PARMELA. (a), (b), and (c) correspond to three locations: after the 238-MHz SHB, after the 476-MHz booster cavity, and before the L-band accelerator, respectively. Part of the energy profile is linearized by the L-band correction rf cavity. The left side of each plot corresponds to the bunch head.

In order to further compress the bunch, three magnetic bunch compressors composed of four dipole magnets having negative R_{56} are used. High-energy electrons take a shorter path than low-energy electrons; thus, the bunch length is shortened. Note that the energy chirp is given by the acceleration in the off-crest phase. The main sources of nonlinearity are the sinusoidal rf field and the higher-order momentum compaction of the magnetic bunch compressors. A C-band correction rf cavity compensates for these nonlinear terms, the frequency of which is the fourth harmonic of the L-band accelerator. The C-band correction cavity was installed upstream of BC1. The nonlinearity is overcorrected so as to linearize the electron bunch after the final bunch compressor, as shown in Fig. 4[12].

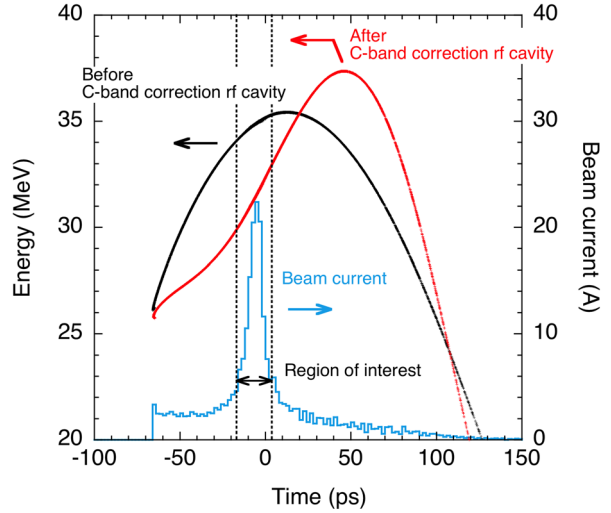

FIG. 4. Energy profile (black and red dots) and beam current (blue line) as functions of the bunch longitudinal position (time), simulated using PARMELA. The left side corresponds to the bunch head. The black and red dots correspond to the locations before and after the C-band correction rf cavity, respectively.

B. Optimization of injector acceleration-structure rf frequency

1. Use of L-band accelerator as main acceleration system

In the SCSS test accelerator, an S-band accelerator was used for the main acceleration in the injector. In general, to compensate for the second-order nonlinearity of such a rf field, a higher-harmonic rf cavity is introduced after the main accelerator; e.g., an X-band (11.4 GHz) correction cavity is typically positioned after an S-band (2.9 GHz) accelerator [15]. However, the rf system becomes technically more complex and expensive with a higher rf frequency. To avoid these problems in the case of SACLA, we decided to use a combination of an L-band (1.4 GHz) accelerator and a C-band (5.7 GHz) correction cavity.

The L-band accelerator has another advantage, in that it prevents the generation of superfluous satellite bunches in the acceleration process. In the SCSS injector, although the electron bunch is longitudinally compressed by the velocity bunching, the full bunch length at the entrance of the S-band structure remains longer than its rf bucket size. Therefore, the tail part of the electron bunch spills from the rf buckets and is captured in the subsequent rf buckets, inducing satellite-bunch generation.

The satellite-bunch generation process in the S-band accelerator of the SCSS injector was simulated using PARMELA. An electron bunch full length of approximately 260 ps was obtained at the entrance of the S-band structure, as shown in Fig. 5(a). To add an energy chirp for the magnetic compression, this bunch is accelerated with an off-crest rf phase. Then, satellite bunches are generated, as shown in Fig. 5(b). These satellite bunches remain even after the BC1 energy slit, as shown in Fig. 5(c). A similar simulation was performed for the L-band accelerator of the SACLA injector. The results are shown in Fig. 6. It was confirmed that the satellite-bunch generation was dramatically reduced by the large L-band rf bucket.

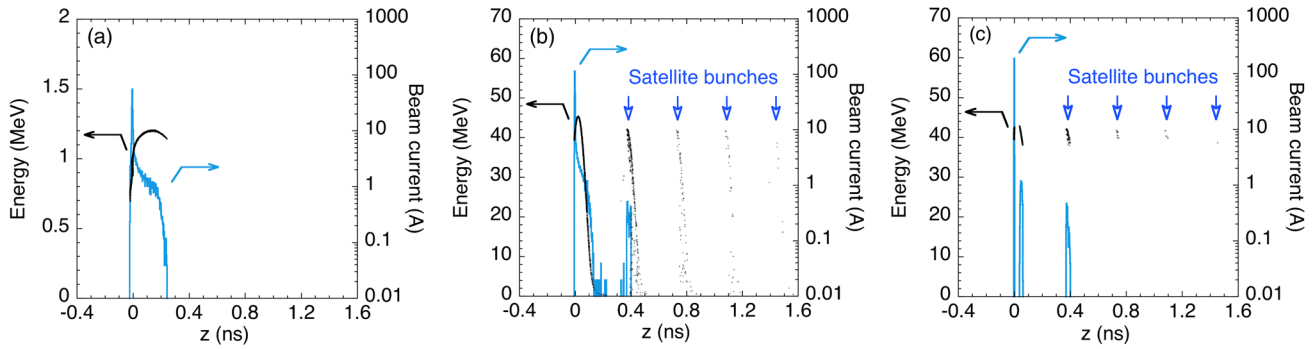

FIG. 5. Energy profile (black dots) and beam current (blue line) as functions of the bunch longitudinal position (time) for the SCSS injector simulated using PARMELA. (a), (b), and (c) correspond to the S-band structure entrance and exit and after the BC1 energy slit, respectively.

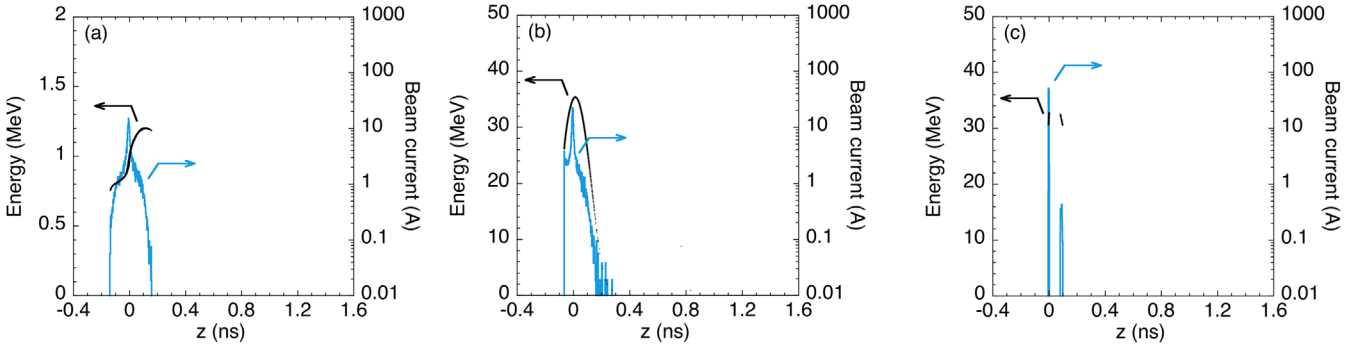

FIG. 6. Energy profile (black dots) and beam current (blue line) as functions of the bunch longitudinal position (time) for the SACLA injector simulated using PARMELA. (a), (b), and (c) correspond to the L-band structure entrance and exit and after the BC1 energy slit, respectively.

2. L-band accelerator system

Two L-band alternative periodic structures (APS) were employed in the SACLA injector. Each of the structures possesses 18 acceleration cells and a rf coupler cell located in the center of the structure. The initial beam energy at the L-band accelerator entrance remains low, at approximately 1 MeV. If a traveling-wave-type structure is used, the asymmetric rf field at the coupler cell distorts the electron beam. On the other hand, a standing-wave-type structure with symmetric rf fields is preferable at this location, considering the emittance preservation. The coupler cell has a dummy port on the opposite side of a lateral iris matched to the waveguide, and correcting field asymmetry is introduced by the iris. Furthermore, the beam passes the coupler cell after acceleration to 7 MeV. Consequently, the beam is not deflected significantly in the structures.

C. rf-system stabilization

1. Stability tolerance determined from particle tracking simulation

As a slight fluctuation of the injector rf parameters hinders precise beam tuning, i.e., with regards to the beam acceleration, bunch compression, and orbit correction (particularly in the undulator section), the injector rf parameters should be highly stabilized and accurately controlled. To obtain stable XFEL operation, the beam peak current fluctuation must be suppressed to within 10%. In order to estimate the stability tolerance of the injector rf cavities, we used a one-dimensional particle tracking simulator [16]. From the simulation results, it was confirmed that the stability tolerances of the amplitude and phase of each rf cavity should be below 100 ppm and 100 fs, respectively, as shown in Table II. These values are less than one-third compared to those of the SCSS injector.

2. Injector rf system overview

Block diagrams of the injector rf system containing the L-band and C-band correction cavities are shown in Fig. 7. The main rf parameters and power sources are summarized in Table III. In SACLA, the rf reference signals are generated by the master oscillator [17]. The signals are distributed to each amplifier through an in-phase and quadrature modulator (IQ MOD), as shown in Fig. 7. The amplitude and phase of each rf cavity are controlled by the IQ MOD with a 16-bit digital-to-analog converter

TABLE II. Stability tolerance and realized performance of SACLA-injector rf components.

Component		Stability tolerance (σ)	Measurement (std)
Gun voltage	Amplitude	0.003%	0.001%
238-MHz subharmonic buncher	Amplitude	0.01%	0.01%
	Phase	0.01°	0.01°
476-MHz booster cavity	Amplitude	0.01%	0.01%
	Phase	0.02°	0.01°
L-band correction cavity	Amplitude	0.03%	0.01%
	Phase	0.06°	0.01°
L-band accelerator	Amplitude	0.01%	0.01%
	Phase	0.06°	0.01°
C-band correction cavity	Amplitude	0.1%	0.02%
	Phase	0.1°	0.1°

(DAC). The rf signals are detected by an IQ detector (IQ DET) with a 16-bit analog to digital converter (ADC), and a waveguide directional coupler and a rf-cavity pick-up port are used to measure the rf amplitude and phase. In a conventional rf measurement, the ADC samples the value at a specific timing of the rf waveform from the IQ DET. However, the rf measurement system can also store the waveform of the rf pulse at 60 Hz. For some important rf signals, which require a higher resolution to facilitate the observation of the slight variation of the rf amplitude and phase, the number of sampling points is increased around the specific timing of the rf waveform, to induce noise reduction. In this case, the resolution is improved by a factor of 3.

3. Techniques to improve injector rf stability

In order to stabilize the injector rf system, countermeasures against various instabilities were considered in the basic design of the SACLA-injector rf components. As a result, the amplitude and phase stabilities satisfy the target tolerance values listed in Table II.

Electric-power variation reduction.—The low-level rf instruments, such as the IQ MODs and IQ DETs, and the solid-state amplifiers are powered by low-noise power-supply devices, which have noise levels of less than -140 dB V/$\sqrt{\text{Hz}}$ between 30 and 400 Hz.

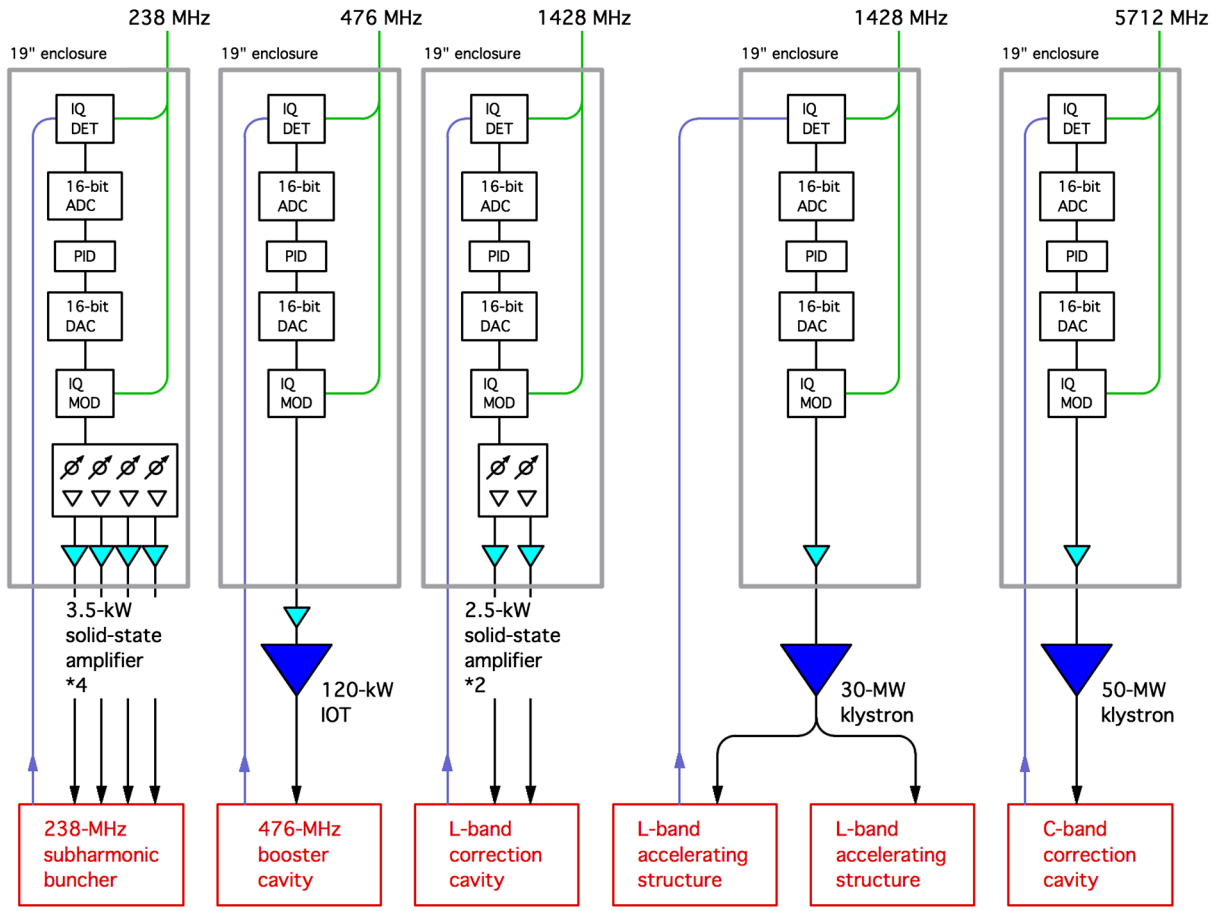

FIG. 7. rf block diagrams of the SACLA injector. IQ MOD and IQ DET indicate the IQ modulator and IQ detector, respectively. PID indicates the proportional-integral-derivative controller. The 476-MHz rf signal is amplified by a 120-kW inductive output tube (IOT).

TABLE III. Main rf parameters of SACLA-injector rf cavities and power sources.

	Subharmonic buncher	Booster cavity	L-band correction cavity	L-band accelerator	C-band correction cavity
Frequency	238 MHz	476 MHz	1428 MHz	1428 MHz	5712 MHz
Cavity type	Standing-wave reentrant	Standing-wave reentrant	Standing-wave reentrant	Standing-wave APS	Traveling-wave constant impedance
Acceleration mode	π	π	π	$\pi/2$	$3\pi/4$
Quality factor	15300	26000	20156	24700	10582
Coupling	1.56	1.66	3.02	1.46	1.5
Shunt impedance	5.94 MΩ	7.8 MΩ	6.68 MΩ	36 MΩ/m	52.4 MΩ/m
Gap voltage, gradient	200 kV	800 kV	140 kV	9.2 MV/m	6.1 MV/m
Number of cells	1	1	1	18 + coupler	26
Length	0.51 m	0.4 m	0.115 m	2 m	0.59 m
Amplifier type	Solid state	IOT	Solid state	Klystron	Klystron
Power (typical)	10 kW	80 kW	2.5 kW	20 MW	4 MW
Pulse width	100 μs	50 μs	10 μs	5 μs	1 μs

Temperature stabilization.—As the IQ MOD and IQ DET performance is temperature dependent, a thermally controlled 19" enclosure is employed in order to maintain a constant environmental temperature for these rf instruments. The temperature variations of the recirculating air inside the enclosure are regulated to within $\pm 0.2°$C (peak to peak, p-p). To suppress the rf phase drift of the transmission lines, such as the optical fibers of the reference rf signals, the coaxial cables, and the waveguides, the temperature variations of those lines are restricted to within ± 0.2 ℃ (p-p) using coolant water and heat insulators. The temperature variation of each rf cavity is restricted to within ± 0.04 ℃ (p-p) with an adjustable range of 27 to 30 ℃ using the precise temperature regulation system of the cooling water [18].

Mechanical vibration suppression.—To suppress the mechanical vibration of the rf cavities due to the coolant-water circulation, the rf cavities are designed to be massive (e.g., the 238-MHz SHB has 720-kg mass), and the water differential pressure of each rf cavity is designed to be below 0.2 MPa. In addition, the injector rf cavities are placed on a stone table composed of gabbro in order to reduce the mechanical vibration. Note that this stone table is also relatively insensitive to temperature changes.

Precise modulator power supply.—In SACLA, pulse modulators using pulse forming network (PFN) circuits are employed as power sources for the 500-kV gun and the L-band [19] and C-band pulse power klystrons [20]. A single-tank design is adopted for the pulse modulators [13]. All high-voltage components, including the PFN circuit, thyratron tube, and pulse transformers, are installed in a steel tank filled with insulation oil. The steel tank functions as an electromagnetic noise shield to contain the thyratron noise. The PFN voltage (50 kV) is charged by an inverter-type high-voltage charger, which has a stability of better than 10 ppm (std).

D. Nondestructive beam diagnostic system for precise parameter monitoring

As the electron-bunch velocity in the upstream part of the injector does not reach the velocity of light, it is useful to measure the time of flight (TOF) in order to check the beam timing stability. Therefore, we prepared three types of diagnostics for TOF measurement.

The TOF between the exit of the 238-MHz SHB and that of the L-band correction cavity was measured from the waveforms of two current transformers (CTs), as shown in Fig. 2. The signals from these two CTs were sent to an oscilloscope having a time-interval measurement function. The measurement resolution at a moving average of 10 points was approximately 0.2 ps.

Three strip-line-type beam position monitors (BPMs) and a cavity-type beam arrival time monitor (BATM) were installed at the locations shown in Fig. 2[21]. The signals from these monitors are measured by the IQ DET with a 16-bit ADC through an amplifier. The measurement resolution at a moving average of 10 points was approximately 30 fs (std). Note that, as these TOF measurements are nondestructive, this behavior can always be observed and monitored during daily operation.

E. Installation of long air-core coils for geomagnetic-field correction

As the beam energy in the upstream part of the injector is lower than 1 MeV, the electron beam orbit can be easily affected by the geomagnetic field. Further, as the electron-bunch beam energy is modulated for the velocity bunching, it is necessary to achieve a straight beam trajectory in order to avoid chromatic effects or dispersion, which causes the projected emittance growth.

In order to compensate for the geomagnetic field, 7-m-long air-cored coils covering the low-energy part of the injector, which extends from the gun to the first L-band

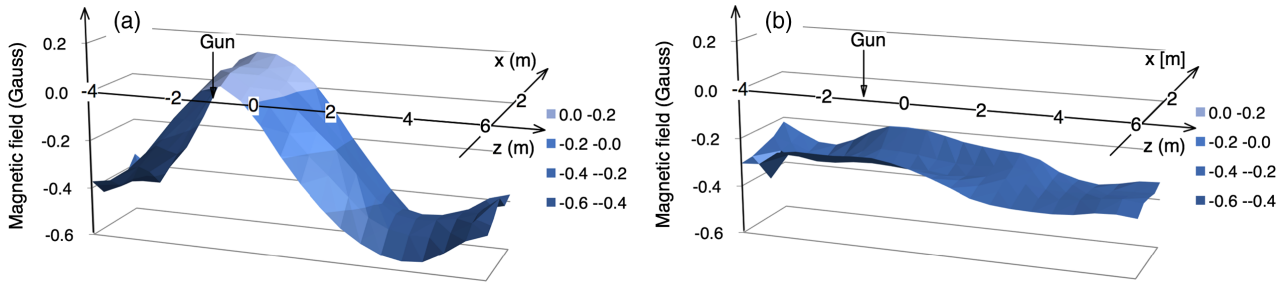

FIG. 8. Vertical magnetic field distribution on the horizontal plane at beam height (800 mm) in the injector area (a) before and (b) after demagnetization.

APS, were employed. We first surveyed the magnetic field around the injector area in the accelerator tunnel, before installing the components. The measured data show that the magnetic field is strongly dependent on the measurement position, as shown in Fig. 8(a). The source of this inhomogeneity is the magnetization of the reinforcing steel buried in the concrete floor.

As this inhomogeneous magnetic field cannot be corrected by a single long coil, which would generate a uniform magnetic field, we demagnetized the reinforcing steel using a flat square coil so as to render the magnetic field uniform [22]. This square coil generates ac magnetic fields with a slowly damping amplitude. The magnetic field distribution after the demagnetization process is shown in Fig. 8(b). The variation of the vertical field is suppressed to within a range of −0.39 to −0.2 G. Before the demagnetization, this variation was −0.56 to 0.13 G.

IV. SACLA-INJECTOR BEAM CHARACTERISTICS

A. Reconstruction of longitudinal bunch profile

In SACLA, the electron-beam energy profile after the injector is measured using a screen monitor located at the energy dispersive part of BC1. The energy profile is obtained from the convolution of the energy dispersion and the natural beam size determined by the beta function and emittance. Note that, as the beam-size contribution is small, it is negligible for the energy-profile measurement. Energy profiles obtained via both measurement and simulation are shown in Fig. 9.

The bunch profile Δt on the longitudinal axis is given by

$$\Delta t = \frac{E}{c \cdot \eta \cdot dE/dz} \Delta x, \tag{1}$$

where E is the beam energy, c is the velocity of light, η is the BC1 energy dispersion, dE/dz is the energy chirp determined by the rf parameters, and Δx is the horizontal size on the screen [23]. In order to obtain the longitudinal charge distribution, the total electron-beam charge at the injector exit is measured by the CT. Figure 10(a) shows the longitudinal charge distribution of the bunch derived from the measured total charge and the energy profile shown in Fig. 9(a). The simulation result obtained at the same location is also shown in Fig. 10(b) for comparison. It is apparent that the observed energy profile and the obtained peak current are in agreement with the simulation results.

For the nominal XFEL operation of SACLA, the central part of the bunch is cut out by the BC1 energy slit. The bunch charge after the slit is 0.3 nC, which corresponds to a 20-ps bunch length and a 20-A peak current, as shown in

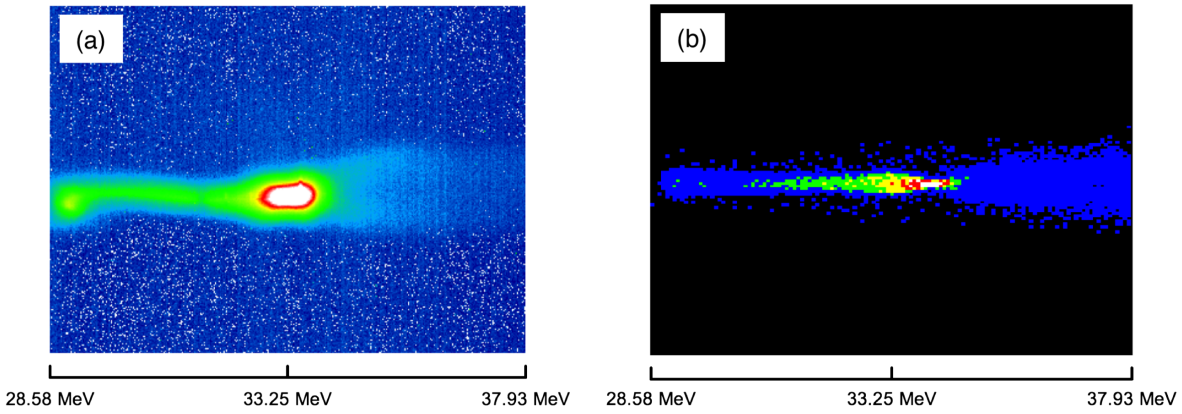

FIG. 9. Energy profiles at energy dispersive part of BC1. (a) Measured and (b) simulated (by PARMELA code) energy profiles at the injector exit.

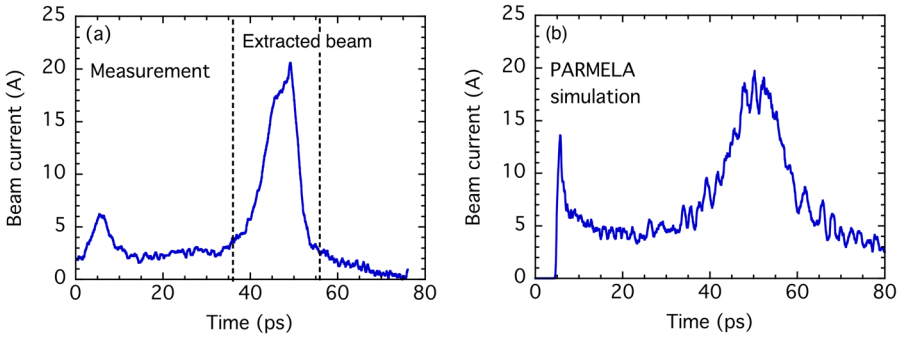

FIG. 10. Longitudinal bunch profiles at the injector exit. (a) Measured longitudinal current distribution at the injector exit. The peak current and bunch length are 20 A and 8.8 ps (FWHM), respectively. (b) Longitudinal current distribution at the injector exit simulated by PARMELA code.

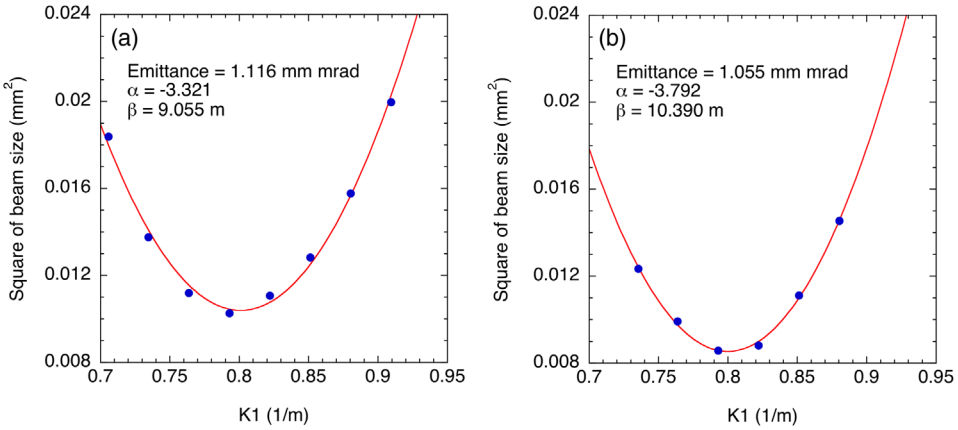

FIG. 11. (a) Horizontal and (b) vertical projected emittances at the BC1 exit measured via a quadrupole scan.

Fig. 10(a). Then, the extracted beam is compressed by BC1, which has a compression factor of approximately 3.

B. Projected emittance measurement

The beam emittance was measured by a quadruple scan method after BC1; the results are shown in Fig. 11. The normalized projected emittance was 1.1 mm mrad (root-mean-square), which is in close agreement with the simulation result. The emittance was improved to one-third that obtained for the SCSS test accelerator because of the straight beam orbit achieved using the long air-cored correction coils.

C. Evaluation of peak current and slice emittance from lasing data

To measure the peak current and to verify the bunch compression linearization, we measured the longitudinal charge distribution of the electron bunches after the third magnetic bunch compressor using rf deflectors [24]. A peak current of 3.5 kA was obtained from analysis of the measured data.

The slice emittance was estimated from the measured FEL gain curve and the peak current of the electron bunch. An example of the gain curve is shown in Fig. 12. Assuming a 3.5-kA peak current, the normalized-slice emittance was estimated to be 0.7 mm mrad [1]. Hence, it was confirmed that the linearization of the bunch compression process in the injector works well without emittance degradation.

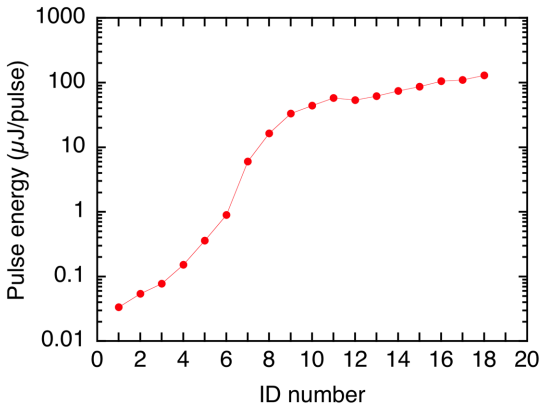

FIG. 12. FEL gain curve at 10-keV photon energy [1]. The photon pulse energy amplification is plotted as a function of the undulator number. The electron beam energy was 7 GeV.

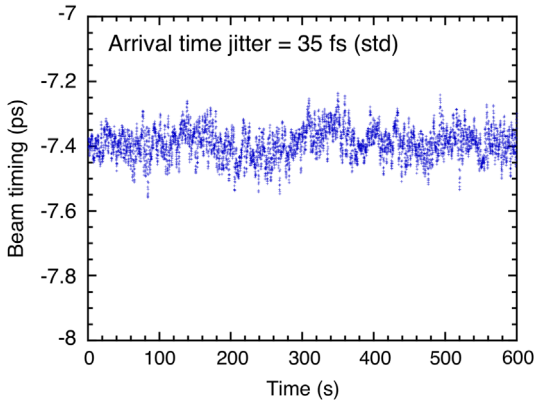

FIG. 13. Beam arrival time jitter measured at the injector exit. The time jitter is 35 fs (std), which satisfies the 50-fs (σ) target limit.

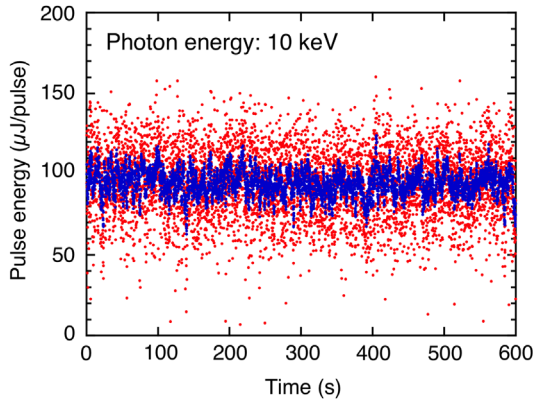

FIG. 14. XFEL pulse energy trend at beam commissioning. The red and blue points correspond to shot-by-shot intensities and the 10-shot moving average, respectively. The photon and electron-beam energies are 10 keV and 7 GeV, respectively.

D. Beam arrival time stability and XFEL intensity

During the machine tuning, which includes the bunch compression and beam orbit correction in the undulators, the stability and reproducibility of the beam in the injector must be maintained in order to optimize the parameters. In particular, the TOF of the electron bunches in the injector should be held constant. If the beam arrival time at the injector exit has a timing jitter larger than the target value shown in Table II, the energy chirp changes and the peak current varies after the magnetic bunch compressor. The stability of the beam arrival time at the injector exit is measured by a rf-cavity-type BATM. Using these data, the measured arrival time jitters were found to be less than 35 fs (std), as shown in Fig. 13. This value satisfies the strict rf phase stability tolerances in the injector.

Because of the good injector-beam reproducibility, the beam tuning proceeded smoothly during the commissioning period. The first lasing was achieved only 3 months after beam commissioning was initiated. The XFEL pulse energy was approximately 100 μJ/pluse with 20% (std) fluctuation, as shown in Fig. 14.

E. Improvement of laser pointing stability

For user experiments, the XFEL beam pointing stability is of considerable importance. When the beam commissioning was initiated, the photon-beam position spread over half its spot size from pulse to pulse. In order to reduce the pointing jitter, we investigated the source of this fluctuation, which was then identified as the beam orbit fluctuation in the injector.

We analyzed the frequency components of the beam position variation in the injector using fast Fourier transform analysis. Figure 15(a) shows the resultant beam position variation spectrum. A peak was observed at 2 Hz, which coincides with the operating cycle of the pulse width modulation current of the precise cooling-water temperature regulation system for the rf cavities. It was found that the beam position in the injector was affected by a slight leakage of the magnetic fields generated by the ac heaters and their cables.

To suppress the magnetic-field leakage from the ac heaters, we replaced these heaters with dc heaters, which

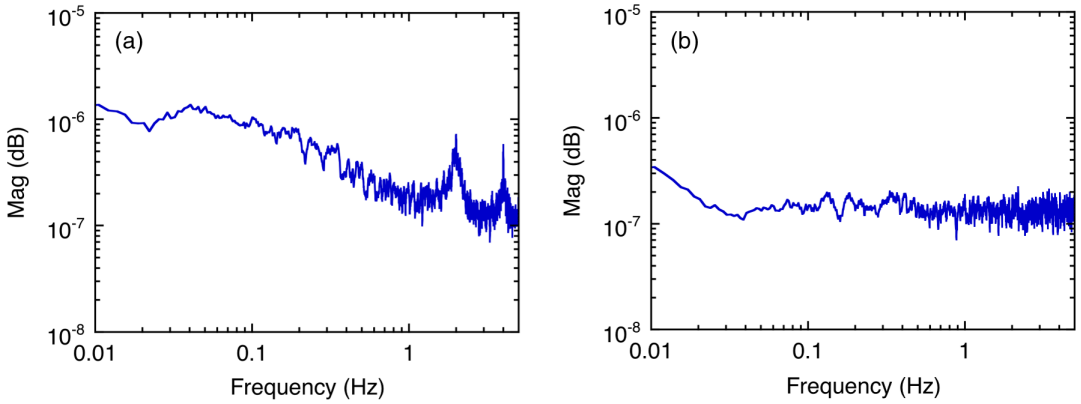

FIG. 15. Spectral analysis results for the vertical beam position after BC1. (a) The frequency of the beam position jitter was observed to be 2 Hz before the modification. (b) The peak at 2 Hz was removed after the modification.

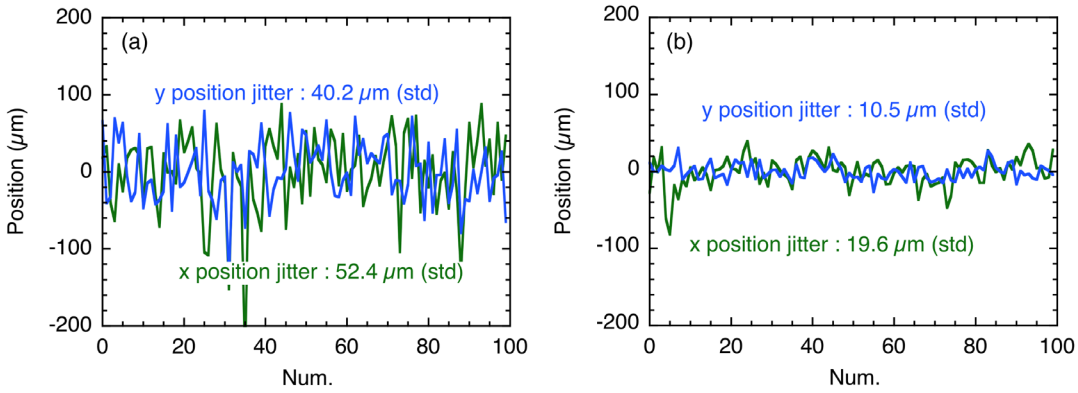

FIG. 16. Laser pointing stability observed 80 m downstream of the undulator exit (a) before and (b) after the heater replacement. The laser position was measured using the beam-line screen monitor.

are driven by a dc power supply. As a result, the beam position variation at 2 Hz and the long-term drift were removed, as shown in Fig. 15(b). In addition, the temperature measurement module with 0.01 °C resolution was replaced with a new module having a resolution of 0.001 °C.

The reduction of the beam position variation in the injector had a remarkable effect on the laser pointing stability. The laser positions observed 80 m downstream of the undulator exit before and after the modification are shown in Fig. 16. The laser-position fluctuations in the horizontal and vertical directions, which were originally 52.4 and 40.2 μm, respectively, were reduced by approximately half and one-quarter, respectively, after the modification. The laser pointing stability was finally reduced to less than 10% (std) of the laser spot size.

V. SUMMARY

To provide a stable XFEL for user experiments, an injector using a low-emittance thermionic-gun has been developed for SACLA based on experience obtained from the design and operation of the SCSS test accelerator. In order to achieve a high bunch compression factor of more than 3000, various modifications have been made to the SACLA injector, such as the installation of L-band accelerators and harmonic rf cavities for nonlinear compensation of the bunch compression process. The stability of the rf system is drastically improved owing to newly introduced monitors and detectors with higher resolution, which facilitate the beam tuning.

Currently, the peak current of the electron beam exceeds 10 kA, and the XFEL pulse energy has been increased to more than 600 μJ with an approximately 10% (std) fluctuation. Thus, the electron beam from the injector has shown sufficient stability and reproducibility for satisfactory operation of SACLA.

ACKNOWLEDGMENTS

The authors thank all staff members of SACLA for their continuous support, especially Dr. N. Kumagai, Dr. T. Ishikawa, Dr. H. Kitamura, and Dr. T. Shintake who have performed management and promotion duties. We also thank Dr. T. Taniuchi for useful discussions relating to the development of the L-band rf components. In addition, the authors also thank Dr. S. Miura and Mr. K. Okihira of Mitsubishi Heavy Industries Ltd., Ms. J. Watanabe of Toshiba Corporation Power Systems Company, and Mr. S. Fujii of Toshiba Electron & Devices Co., Ltd., for practical engineering work and production execution of excellent quality. We gratefully acknowledge the help and support of the SPring-8 service company staff.

[1] T. Ishikawa *et al.*, A compact X-ray free-electron laser emitting in the sub-ångström region, Nat. Photonics **6**, 540 (2012).

[2] T. Shintake *et al.*, SPring-8 compact SASE source (SCSS), in *Proceedings of SPIE, Optics for Fourth-Generation X-ray Sources* (SPIE, Bellingham, WA, 2001), Vol. 4500, p. 12.

[3] SCSS X-FEL R&D Group, *SCSS X-FEL Conceptual Design Report*, edited by T. Tanaka and T. Shintake (RIKEN Harima Institute/SPring-8, Sayo, Japan, 2005).

[4] H. Kitamura, Insertion devices for third-generation light sources, Rev. Sci. Instrum. **66**, 2007 (1995).

[5] T. Shintake *et al.*, C-band linac rf-system for e^+e^- linear collider, in *Proceedings of the Particle Accelerator Conference, Dallas, TX, 1995* (IEEE, New York, 1995), p. 1099.

[6] M. Ferrario and T. Shintake, High performance electron injectors, Rev. Accel. Sci. Techol. **03**, 221 (2010).

[7] D. L. Webster, Cathode-Ray Bunching, J. Appl. Phys. **10**, 501 (1939).

[8] T. Tanaka *et al.*, Status of R&Ds for SCSS project, in *Proceedings of FEL 2005, Palo Alto, California* (JACoW, Geneva, 2005), p. 75.

[9] T. Shintake *et al.*, Status of the SCSS test accelerator and XFEL project in Japan, in *Proceedings of the 10th European Particle Accelerator Conference, Edinburgh, Scotland, 2006* (EPS-AG, Edinburgh, Scotland, 2006), p. 2741.

[10] T. Shintake *et al.*, A compact free-electron laser for generating coherent radiation in the extreme ultraviolet region, Nat. Photonics **2**, 555 (2008).

[11] T. Shintake *et al.*, Stable operation of a self-amplified spontaneous-emission free-electron laser in the extremely ultraviolet region, Phys. Rev. ST Accel. Beams **12**, 070701 (2009).

[12] K. Togawa, T. Hara, and H. Tanaka, Electron-bunch compression using a dynamical nonlinearity correction for a compact x-ray free-electron laser, Phys. Rev. ST Accel. Beams **12**, 080706 (2009).

[13] T. Inagaki, C. Kondo, H. Maesaka, T. Ohshima, Y. Otake, T. Sakurai, K. Shirasawa, and T. Shintake, High-gradient C-band linac for a compact x-ray free-electron laser facility, Phys. Rev. ST Accel. Beams **17**, 080702 (2014).

[14] K. Togawa, T. Shintake, T. Inagaki, K. Onoe, T. Tanaka, H. Baba, and H. Matsumoto, CeB_6 electron gun for low-emittance injector, Phys. Rev. ST Accel. Beams **10**, 020703 (2007).

[15] R. Akre *et al.*, Commissioning the linac coherent light source injector, Phys. Rev. ST Accel. Beams **11**, 030703 (2008).

[16] H. Tanaka *et al.*, Bunch length variation and timing jitter caused by rf system instability in XFEL/SPring-8, in *Proceedings of the 4th Annual Meeting of PASJ* (Particle Accelerator Society of Japan, Tokyo, 2007), p. 613, in Japanese.

[17] Y. Otake, H. Maesaka, S. Matsubara, N. Hosoda, and T. Ohshima, Timing and low-level rf system for an x-ray laser,, Phys. Rev. ST Accel. Beams **19**, 022001 (2016).

[18] T. Hasegawa *et al.*, Status of a precise temperature-regulation system for the C-band accelerator at XFEL/SPring-8, in *Proceedings of the International Particle Accelerator Conference, Kyoto, Japan* (ICR, Kyoto, 2010), p. 1488.

[19] S. Fujii *et al.*, Development of 30 MW L-band pulse klystron for XFEL, in *Proceedings of the 7th Annual Meeting of PASJ* (Particle Accelerator Society of Japan, Himeji, 2010), p. 902, in Japanese.

[20] T. Shintake *et al.*, Development of C-band 50 MW pulse klystron for e^+e^- linear collider, in *Proceedings of the Particle Accelerator Conference, Vancouver, BC, Canada, 1997* (IEEE, New York, 1997), p. 533.

[21] Y. Otake, H. Maesaka, S. Matsubara, S. Inoue, K. Yanagida, H. Ego, C. Kondo, T. Sakurai, T. Matsumoto, and H. Tomizawa, Beam monitor system for an x-ray free electron laser and compact laser, Phys. Rev. ST Accel. Beams **16**, 042802 (2013).

[22] S. Matsui *et al.*, Earth magnetic field and demagnetization of steel structure in the XFEL accelerator tunnel, in *Proceedings of the 7th Annual Meeting of PASJ* (Particle Accelerator Society of Japan, Himeji, 2010), p. 268, in Japanese.

[23] L. Rivkin *et al.*, Bunch lengthening in the SLC damping ring, in *Proceedings of EPAC'88, Rome, Italy,* (JACoW, Geneva, 1988), p. 634.

[24] H. Ego, H. Maesaka, T. Sakurai, Y. Otake, T. Hashirano, and S. Miura, Transverse C-band deflecting structure for longitudinal electron-bunch-diagnosis in XFEL "SACLA, Nucl. Instrum. Methods Phys. Res., Sect. A **795**, 381 (2015).